Novel Detection Methodology of Milk-Oligopeptides Fingerprints using Ion-Sensitive BioFET

Naveen Kumar [a,*], César Pascual García [b,*], Ankit Dixit [a], Ali Rezaei [a], Vihar Georgiev [a,*]
[a] Device Modelling Group, James Watt School of Engineering, University of Glasgow, UK
[b] Nano-Enabled Medicine and Cosmetics Group, Materials Research and Technology Department, Luxembourg Institute of Science and Technology (LIST), Belvaux, Luxembourg
[*] naveen.kumar@glasgow.ac.uk, [*] cesar.pascual@list.lu, ankit.dixit@glasgow.ac.uk, ali.rezaei@glasgow.ac.uk, [*] vihar.georgiev@glasgow.ac.uk

***Abstract*—Protein sequencing is an important key to personalized medicines, but the process is complex enough to halt the ongoing progress in proteomics. In this paper, we have proposed a novel simulation methodology for the detection of oligopeptide fingerprints using a Field-Effect-Transistor. In our approach, the Gouy-Chapman-Stern and Site-Binding models are solved self-consistently to capture the response of immobilized peptides in the presence of an electrolyte. Our results show the unique signatures of two anti-hypertensive tripeptides in terms of variation in surface potential, inflection points and point-of-zero-charge in 2nd order differentiation of surface potential and total surface capacitance. We have shown that the presence of silanol sites, in the presence of single or multiple oligopeptides, is responsible for reduced sensor's sensitivity. We have proposed a novel noise-reduction technique to eliminate the noise present in the experimental data.**

I. Introduction

Several modifications are made to Field-Effect Transistors (FETs) to build the platform for further advancements in biosensors [1]–[12]. Ion-sensitive (IS) FET is the simplest structure for sensing applications [13]–[16]. There are several ISFET architectures [17]–[19] used to tune the sensing parameters but using them for biosensing is limited by the Debye length [20]–[22]. The idea of sensing proteins using FETs was proposed by P. Bergveld [6], [23], [24] but it was discarded as the protein charges reside over the Debye length which are balanced by the counterions in the electrolyte making the sensor insensitive to the immobilized proteins. However, amino acids (AAs) and oligopeptides can be sensed due to their short length keeping the Debye screening within acceptable limits of ionic concentration [25]–[29].

In this work, to show the proof of concept, we have considered two anti-hypertensive tripeptides Isoleucine-Proline-Proline (IPP) and Leucine-Lysine-Proline (LKP) derived from milk β-casein [30]. The FET sensor is immersed in an electrolyte with SiO_2 as the gate oxide. (3-Aminopropyl)triethoxysilane (APTES) is deposited on SiO_2 as a linker to facilitate the immobilization of the oligopeptides [29], [31], [32]. The presence of linker [1], [8], [11] and non-specific binding [1]–[3], [5], [10] can be extracted by calibrating the sensor. The variation in device behavior is captured by analyzing the parameters such as surface potential (Ψ_o), 2nd gradient of Ψ_o ($d^2\Psi_o/dpH^2$) and total surface capacitance (C_T).

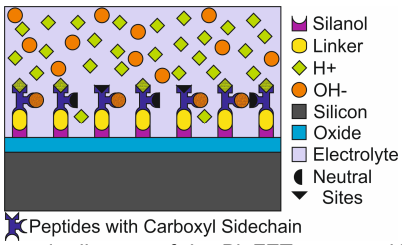

Figure 1. Schematic diagram of the BioFET sensor with immobilized oligopeptides over the oxide. The top of a silanol group is covered with yellow color which is the linker. Oligopeptides have the possibility to be protonated/deprotonated due to active sites (for the receptors).

II. Methodology

The novel analytical model, used here, to analyze oligopeptides sensing is based on the self-consistent solution of Gouy-Chapman-Stern and Site-Binding model (SB) [33]–[35]. SB model explains the probability of the immobilized oligopeptides on the oxide surface resulting in terms of surface charge density (σ_o). σ_o depends on the active surface states (N_S), bulk pH (pH_B) and dissociation constants (K_a, K_b, K_c & K_d) of the active sites present on the oligopeptides [15], [36]–[38]. Here, we have used 5 combinations of both tripeptides immobilized by Carboxylic terminal (C-Imm.) to account for the addition, substitution, and mutation of the considered tripeptides. Every combination corresponds to a different σ_o considering the active sites (amine site (N) and sidechains) [IPP (σ_{o1}), RIPP (σ_{o3}), DPP (σ_{o2}), RDPP (σ_{o4}), LKP (σ_{o3}), RLKP (σ_{o5}), DKP (σ_{o4}), RDKP (σ_{o6}) where R: Arginine & D: Aspartic Acid] except the affinity of the carboxylic terminal reacted in the immobilization with APTES.

$$\sigma_{o1} = qN_S\left(\frac{cH_S}{cH_S + K_a}\right) \quad (1) \qquad \sigma_{o2} = qN_S\left(\frac{cH_S^2 - K_aK_b}{cH_S^2 + cH_S K_a + K_aK_b}\right) \quad (2)$$

$$\sigma_{o3} = qN_S\left(\frac{cH_S^2 + cH_S K_a}{cH_S^2 + cH_S K_a + K_aK_b}\right) \quad (3)$$

$$\sigma_{o4} = qN_S\left(\frac{cH_S^3 + cH_S^2K_a - K_aK_bK_c}{cH_S^3 + cH_S^2K_a + cH_S K_aK_b + K_aK_bK_c}\right) \quad (4)$$

$$\sigma_{o5} = qN_S\left(\frac{cH_S^3 + cH_S^2K_a + cH_S K_aK_b}{cH_S^3 + cH_S^2K_a + cH_S K_aK_b + K_aK_bK_c}\right) \quad (5)$$

$$\sigma_{o6} = qN_S\left(\frac{cH_s^4 + cH_s^3K_a + cH_s^2K_aK_b - K_aK_bK_cK_d}{cH_s^4 + cH_s^3K_a + cH_s^2K_aK_b + cH_sK_aK_bK_c + K_aK_bK_cK_d}\right) \quad (6)$$

Where, $(K_a>K_b>K_c>K_d)$, $cH_s\left(cH_s = cH_B exp\frac{-\Psi_0}{2V_T}\right)$ & cH_B $(cH_B = 10^{-pH_B})$ are the surface and bulk proton concentration respectively and V_T is the thermal voltage. Ψ_o is calculated by

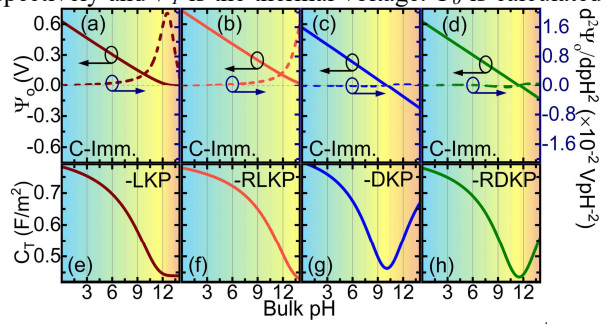

Figure 4. (a) to (e) Surface Potential (Ψ_o) (solid line) and 2nd Gradient of Surface Potential ($d\Psi_o^2/dpH^2$) (dashed line) (f) to (j) Total Capacitance of ISFET with respect to the pH for Carboxy-terminal immobilized for LKP, DLKP, DKP and RDKP respectively. [Assumed 100% coverage]. The difference in Ψ_0 dials down with same proportion for lower surface coverage

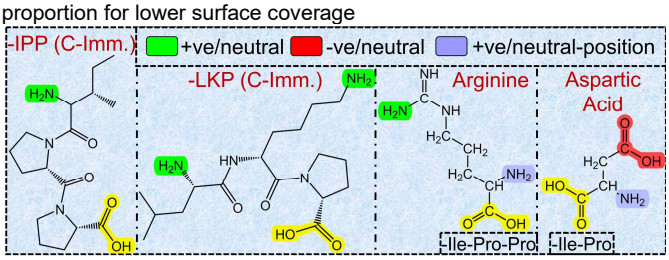

Figure 2. Structures of the used tripeptides (Ile-Pro-Pro and Leu-Lys-Pro) and additional amino acids (Arginine (R) and Aspartic Acid (D)). R is joined with tripeptides by the carboxylic group (yellow) to form tetrapeptides. R is joined with dipeptides (-PP & -KP) by the carboxylic group (yellow) to form tripeptides. If the position of D is 2nd/3rd in the sequence of tri/tetrapeptide, it is joined by both carboxylic (yellow) and amine groups (light purple)

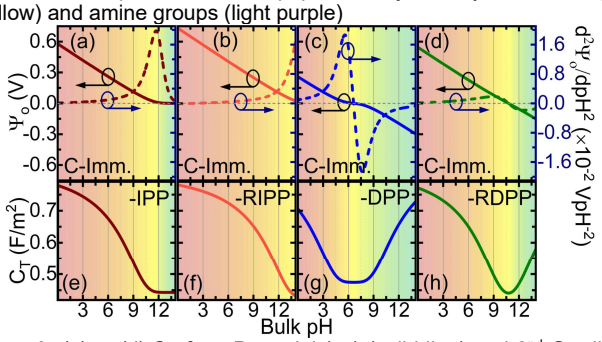

Figure 3. (a) to (d) Surface Potential (Ψ_o) (solid line) and 2nd Gradient of Surface Potential ($d\Psi_o^2/dpH^2$) (dashed line) (e) to (h) Total Capacitance (C_T) of ISFET with respect to the pH for Carboxy-terminal immobilized for IPP, RIPP, DPP and RDPP respectively. [Assumed 100% coverage]. The difference in Ψ_0 dials down with same proportion for lower surface coverage

equating the σ_o with the double-layer charge density (σ_{DL}) from GCS model and the charge density in the semiconducting channel while considering a constant Stern capacitance (C_{stern}) of 0.8 Fm^{-2} [33].

$$\Psi_o = \Psi_{Stern} + \Psi_\xi = \frac{\sigma_{DL}}{C_{stern}} + \Psi_\xi = \frac{Q_0\,sinh(\Psi_\xi/V_T)}{C_{stern}} + \Psi_\xi \quad (7)$$

Where Ψ_ξ represents the zeta potential (at the shear plane).

III. Results

FET sensor is fully depleted at the lowest pH by setting a constant reference bias and it starts conducting with an increase in pH. The C_T is the series combination of the double-layer capacitance, C_{stern} and effective capacitance of the oligopeptides [25], [26]. Figure 1 schematically shows the

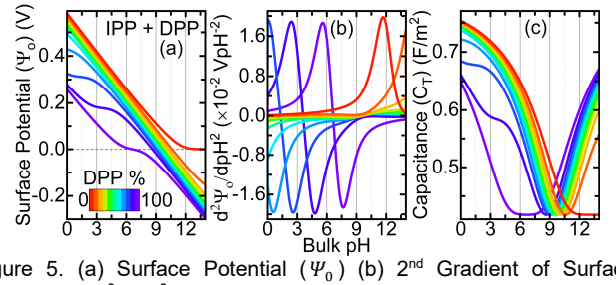

Figure 5. (a) Surface Potential (Ψ_0) (b) 2nd Gradient of Surface Potential ($d\Psi_o^2/dpH^2$) (c) Total capacitance (C_T) Vs pH. Graphs shown for different % of DPP in presence of IPP. Note- IPP population varies with the change in surface coverage by DPP (keeping N_S constant)

molecular arrangement at the FET interface with deposited linker and immobilized oligopeptides immersed in an electrolyte. Figure 2 shows the details of the molecular structure of the peptides (IPP & LKP) with Amine (highlighted green and purple) and carboxylic sites (highlighted red) responsible for positive and negative charges of the oligopeptides. In our simulation, we considered R and D AAs joined either by the carboxylic terminal (yellow) or by both carboxylic and amine (light purple) terminals depending on the position in the sequence. Considering the linker, the presence of APTES shifts the surface potential to more alkaline values due to the higher affinity of amine sites to get protonated resulting in a better sensitivity at lower pH. Our analytical model successfully captures the effect of deposited APTES with and without the presence of silanol sites.

A. *Sensing oligopeptides fingerprints*

The addition of R to tripeptide combinations (IPP→RIPP [Fig. 3(a)→(b)], DPP→RDPP [Fig. 3(c)→(d)], LKP→RLKP [Fig. 4(a)→(b)], DKP→RDKP [Fig. 4(c)→(d)]) shifts the surface potential and C_T to the more alkaline values due to higher protonation affinity of the extra amine sidechain which keeps the oligopeptide positively charged at pH greater than the pK of the original reactive sites. The substitution of I & L with D at the 1st position in the tripeptide sequence (IPP→DPP [Fig. 3(a)→(c)], LKP→DKP [Fig. 4(a)→(c)]) and 2nd position in the tetrapeptide sequence (RIPP→RDPP [Fig. 3(b)→(d)], RLKP→RDKP [Fig. 4(b)→(d)]) can be differentiated due to a carboxylic sidechain with a higher affinity of deprotonation leading to a negative charge on the oligopeptides, in the presence of pH_{pzc} and C_T minima at pH_{pzc}. The zero crossover point of $d^2\Psi_o/dpH^2$ [Fig. 3 and Fig. 4 (c), (d)] and the C_T minima [Fig. 3 and Fig. 4 (g), (h)] represent the isoelectric point associated with the neutral oligopeptides. Without the presence of D, the oligopeptide combinations don't exhibit isoelectric point (or C_T minima) as the amine sites don't have an affinity to acquire negative charge within the pH range.

B. *Unique fingerprints of multiple oligopeptides*

For the detection of multiple oligopeptides, we have assumed the presence of DPP (derivative of IPP) with IPP immobilized over the same oxide surface. We have varied the percentage of DPP while keeping the N_S constant. Even with a slight increase in DPP, the surface potential starts exhibiting the pH_{pzc} due to the carboxylic sidechain of D [Fig. 5(a)]. DPP starts becoming more dominant by showing the saturated

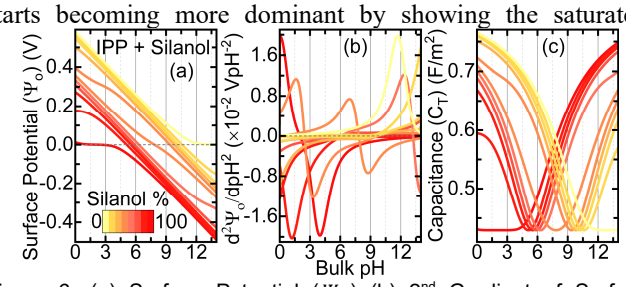

Figure 6. (a) Surface Potential (Ψ_0) (b) 2nd Gradient of Surface Potential ($d\Psi_o^2/dpH^2$) (c) Total capacitance (C_T) Vs pH. Graphs shown for different % of silanol sites in presence of IPP. Note- IPP population also varies with the change in surface coverage by silanol sites

transition with lower sensitivity after it reaches more than 50% as shown in $d^2\,\Psi_o/dpH^2$ [Fig. 5(b)]. C_T shifts towards acidic pH values with increasing DPP population highlighting the C_T minima as compared to the IPP [Fig. 5(c)]. The variation of amplitude, inflection points and pH_{pzc} shift for higher DPP populations constitute the unique fingerprints for detection.

C. *Effect of Silanol Sites*

The presence of silanol sites can vary the reference point of the measured signal leading to hampering the detection of the biomolecule's actual signal. Thus, with an increase in the population of the silanol sites in presence of IPP, the Ψ_o shifts towards the left-hand side, as shown for $2<pH_{pzc}<14$ in Fig. 6(a). The amplitude of minima and maxima points of $d^2\,\Psi_o/dpH^2$ clarifies the transition or saturation of charges with the increase in silanol sites [Fig. 6(b)]. The charge saturation/transition can be observed in FET sensor output between the inflection points for silanol sites close to 50% whereas for the silanol population close to 10% or 90% can be differentiated by the change in drain current amplitude across the PH range. Similarly, to the potential the C_T minima shift towards lower pH values (left-hand side) with the increase of the silanol sites mimicking the pH_{pzc} [Fig. 6(c)].

D. *Noise reduction*

Noise, due to the random motion of the ions in the electrolyte alters the original signal. Here, we have used the analytical model, as a reference, to filter out the noise much better as compared to the moving mean, Savitzky–Golay and traditional Fast-Fourier filtering. The simulated signal (SS) is subtracted from the noisy signal (NS) [Fig. 7(a)] to be assumed as the noise which is filtered from the NS. The filtered noise is compared with the noise extracted [Fig. 7(b)] from the next iteration with a different SS and the same NS. The extracted signal from the NS agrees with the simulated data even when the SNR is 10dB (Fig. 7(c)). The maximum power spectral density of the extracted noise (threshold) [Fig. 7(d)] decreases

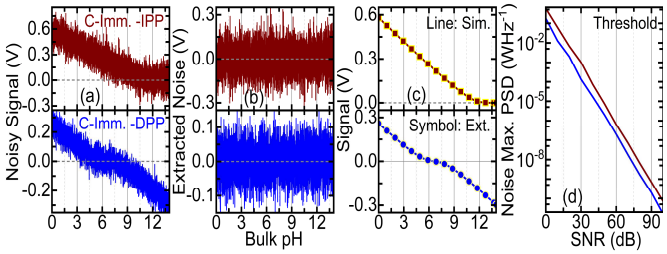

Figure 7. (a) Noisy Signal (NS) (b) Extracted Noise (c) Simulated and Extracted Signal with respect to pH for SNR=10dB and (d) Max. Power Spectral Density (PSD) as the threshold to filter the noise with the variation of SNR for C-Imm. IPP and DPP

with the increase in SNR of the NS (measured) which is different for every oligopeptide combination.

IV. Conclusion

In this work, we have presented an analytical model that allows us to detect unique fingerprints of oligopeptides using potential and capacitance in FET based sensor. These unique signatures allow us to differentiate between oligopeptides or any possible change (mutations) in the sequence of the oligopeptide itself. Moreover, the developed model can extract the population of a single short peptide even in the presence of other oligopeptides in the solution. The effect of silanol sites, on the sensor surface, in the presence of oligopeptides, is also studied. Such simulation results provide a solution to extract the actual signal and linearize the sensor output. We have developed further the simulation methodology by considering noise in the system. We have proposed a novel noise reduction technique that can help us to filter out the noise while pinpointing the fingerprints which can be used as parallel processing of experimental signals in measuring instruments.

References

[1] D. Kwong Hong Tsang *et al.*, "Chemically Functionalised Graphene FET Biosensor for the Label-free Sensing of Exosomes," *Sci Rep*, vol. 9, no. 1, p. 13946, 2019, doi: 10.1038/s41598-019-50412-9.

[2] M.-Y. Shen, B.-R. Li, and Y.-K. Li, "Silicon nanowire field-effect-transistor based biosensors: From sensitive to ultra-sensitive," *Biosens Bioelectron*, vol. 60, pp. 101–111, 2014, doi: https://doi.org/10.1016/j.bios.2014.03.057.

[3] Y. Chen *et al.*, "Field-Effect Transistor Biosensor for Rapid Detection of Ebola Antigen," *Sci Rep*, vol. 7, no. 1, p. 10974, 2017, doi: 10.1038/s41598-017-11387-7.

[4] J. Basu and C. RoyChaudhuri, "Attomolar Sensitivity of FET Biosensor Based on Smooth and Reliable Graphene Nanogrids," *IEEE Electron Device Letters*, vol. 37, no. 4, pp. 492–495, 2016, doi: 10.1109/LED.2016.2526064.

[5] S. Mao, K. Yu, J. Chang, D. A. Steeber, L. E. Ocola, and J. Chen, "Direct Growth of Vertically-oriented Graphene for Field-Effect Transistor Biosensor," *Sci Rep*, vol. 3, no. 1, p. 1696, 2013, doi: 10.1038/srep01696.

[6] P. Bergveld, "The development and application of FET-based biosensors," *Biosensors (Basel)*, vol. 2, no. 1, pp. 15–33, 1986, doi: https://doi.org/10.1016/0265-928X(86)85010-6.

[7] Q. Li, N. Lu, L. Wang, and C. Fan, "Advances in Nanowire Transistor-Based Biosensors," *Small Methods*, vol. 2, no. 4, p. 1700263, Apr. 2018, doi: https://doi.org/10.1002/smtd.201700263.

[8] M. A. Zamzami *et al.*, "Carbon nanotube field-effect transistor (CNT-FET)-based biosensor for rapid detection of SARS-CoV-2 (COVID-19) surface spike protein S1," *Bioelectrochemistry*, vol. 143, p. 107982, 2022, doi: https://doi.org/10.1016/j.bioelechem.2021.107982.

[9] D. Moon, J. Han, and M. Meyyappan, "Comparative Study of Field Effect Transistor Based Biosensors," *IEEE Trans Nanotechnol*, vol. 15, no. 6, pp. 956–961, 2016, doi: 10.1109/TNANO.2016.2615855.

[10] Y. Chen, R. Ren, H. Pu, J. Chang, S. Mao, and J. Chen, "Field-effect transistor biosensors with two-dimensional black phosphorus nanosheets," *Biosens Bioelectron*, vol. 89, pp. 505–510, 2017, doi: https://doi.org/10.1016/j.bios.2016.03.059.

[11] T.-T. Tran and A. Mulchandani, "Carbon nanotubes and graphene nano field-effect transistor-based biosensors," *TrAC Trends in Analytical Chemistry*, vol. 79, pp. 222–232, 2016, doi: https://doi.org/10.1016/j.trac.2015.12.002.

[12] M. S. Makowski and A. Ivanisevic, "Molecular Analysis of Blood with Micro-/Nanoscale Field-Effect-Transistor Biosensors," *Small*, vol. 7, no. 14, pp. 1863–1875, Jul. 2011, doi: https://doi.org/10.1002/smll.201100211.

[13] S. Martinoia, G. Massobrio, and L. Lorenzelli, "Modeling ISFET microsensor and ISFET-based microsystems: a review," *Sens Actuators B Chem*, vol. 105, no. 1, pp. 14–27, 2005, doi: https://doi.org/10.1016/j.snb.2004.02.046.

[14] B. H. van der Schoot and P. Bergveld, "ISFET based enzyme sensors," *Biosensors (Basel)*, vol. 3, no. 3, pp. 161–186, 1987, doi: https://doi.org/10.1016/0265-928X(87)80025-1.

[15] G. A. J. Besselink, R. B. M. Schasfoort, and P. Bergveld, "Modification of ISFETs with a monolayer of latex beads for specific detection of proteins," *Biosens Bioelectron*, vol. 18, no. 9, pp. 1109–1114, 2003, doi: https://doi.org/10.1016/S0956-5663(02)00243-9.

[16] K. B. Parizi, X. Xu, A. Pal, X. Hu, and H. S. P. Wong, "ISFET pH Sensitivity: Counter-Ions Play a Key Role," *Sci Rep*, vol. 7, no. 1, p. 41305, 2017, doi: 10.1038/srep41305.

[17] W. Wei, Z. Zeng, W. Liao, W. K. Chim, and C. Zhu, "Extended Gate Ion-Sensitive Field-Effect Transistors Using Al2O3/Hexagonal Boron Nitride Nanolayers for pH Sensing," *ACS Appl Nano Mater*, vol. 3, no. 1, pp. 403–408, Jan. 2020, doi: 10.1021/acsanm.9b02037.

[18] H.-J. Jang and W.-J. Cho, "Performance Enhancement of Capacitive-Coupling Dual-gate Ion-Sensitive Field-Effect Transistor in Ultra-Thin-Body," *Sci Rep*, vol. 4, no. 1, p. 5284, 2014, doi: 10.1038/srep05284.

[19] S. Rollo, D. Rani, R. Leturcq, W. Olthuis, and C. Pascual García, "High Aspect Ratio Fin-Ion Sensitive Field Effect Transistor: Compromises toward Better Electrochemical Biosensing," *Nano Lett*, vol. 19, no. 5, pp. 2879–2887, May 2019, doi: 10.1021/acs.nanolett.8b04988.

[20] V. Kesler, B. Murmann, and H. T. Soh, "Going beyond the Debye Length: Overcoming Charge Screening Limitations in Next-Generation Bioelectronic Sensors," *ACS Nano*, vol. 14, no. 12, pp. 16194–16201, Dec. 2020, doi: 10.1021/acsnano.0c08622.

[21] I. M. Bhattacharyya and G. Shalev, "Electrostatically Governed Debye Screening Length at the Solution-Solid Interface for Biosensing Applications," *ACS Sens*, vol. 5, no. 1, pp. 154–161, Jan. 2020, doi: 10.1021/acssensors.9b01939.

[22] F. Pittino, P. Palestri, P. Scarbolo, D. Esseni, and L. Selmi, "Models for the use of commercial TCAD in the analysis of silicon-based integrated biosensors," *Solid State Electron*, vol. 98, pp. 63–69, 2014, doi: https://doi.org/10.1016/j.sse.2014.04.011.

[23] P. Bergveld, "A critical evaluation of direct electrical protein detection methods," *Biosens Bioelectron*, vol. 6, no. 1, pp. 55–72, 1991, doi: https://doi.org/10.1016/0956-5663(91)85009-L.

[24] P. Bergveld, R. van Hal, and J. Eijkel, "The remarkable similarity between the acid-base properties of ISFETs and proteins and the consequences for the design of ISFET biosensors," 1995.

[25] S. Zhang, J. Ding, Y. Liu, J. Kong, and O. Hofstetter, "Development of a Highly Enantioselective Capacitive Immunosensor for the Detection of α-Amino Acids," *Anal Chem*, vol. 78, no. 21, pp. 7592–7596, Nov. 2006, doi: 10.1021/ac060840h.

[26] M. Wu, W. Li, S. Li, and G. Feng, "Capacitive performance of amino acid ionic liquid electrolyte-based supercapacitors by molecular dynamics simulation," *RSC Adv*, vol. 7, no. 46, pp. 28945–28950, 2017, doi: 10.1039/C7RA00443E.

[27] T. Civitarese and G. Zollo, "Triggering Amino Acid Detection by Atomistic Resolved Tunneling Current Signals in Graphene Nanoribbon Devices for Peptide Sequencing," *ACS Appl Nano Mater*, vol. 4, no. 1, pp. 363–371, Jan. 2021, doi: 10.1021/acsanm.0c02720.

[28] L. Li *et al.*, "A Bio-inspired Extended-Gate Metal-Oxide-Semiconductor Field-Effect-Transistor for Highly Sensitive Amino Acid Enantiodiscrimination," *Anal Chem*, vol. 93, no. 43, pp. 14425–14431, Nov. 2021, doi: 10.1021/acs.analchem.1c02460.

[29] M. Hatada, T.-T. Tran, W. Tsugawa, K. Sode, and A. Mulchandani, "Affinity sensor for haemoglobin A1c based on single-walled carbon nanotube field-effect transistor and fructosyl amino acid binding protein," *Biosens Bioelectron*, vol. 129, pp. 254–259, 2019, doi: https://doi.org/10.1016/j.bios.2018.09.069.

[30] J. P. Gleeson, J. Heade, S. M. Ryan, and D. J. Brayden, "Stability, toxicity and intestinal permeation enhancement of two food-derived antihypertensive tripeptides, Ile-Pro-Pro and Leu-Lys-Pro," *Peptides (N.Y.)*, vol. 71, pp. 1–7, Jun. 2015, doi: 10.1016/j.peptides.2015.05.009.

[31] Y. Liang, J. Huang, P. Zang, J. Kim, and W. Hu, "Molecular layer deposition of APTES on silicon nanowire biosensors: Surface characterization, stability and pH response," *Appl Surf Sci*, vol. 322, pp. 202–208, 2014, doi: https://doi.org/10.1016/j.apsusc.2014.10.097.

[32] T.-M. Pan *et al.*, "Rapid and label-free detection of the troponin in human serum by a TiN-based extended-gate field-effect transistor biosensor," *Biosens Bioelectron*, vol. 201, p. 113977, 2022, doi: https://doi.org/10.1016/j.bios.2022.113977.

[33] R. E. G. van Hal, J. C. T. Eijkel, and P. Bergveld, "A novel description of ISFET sensitivity with the buffer capacity and double-layer capacitance as key parameters," *Sens Actuators B Chem*, vol. 24, no. 1, pp. 201–205, 1995, doi: https://doi.org/10.1016/0925-4005(95)85043-0.

[34] R. E. G. van Hal, J. C. T. Eijkel, and P. Bergveld, "A general model to describe the electrostatic potential at electrolyte oxide interfaces," *Adv Colloid Interface Sci*, vol. 69, no. 1, pp. 31–62, 1996, doi: https://doi.org/10.1016/S0001-8686(96)00307-7.

[35] R. Dhar, N. Kumar, C. Pascual Garcia, and V. Georgiev, "Assessing the Effect of Scaling High-Aspect-Ratio ISFET with Physical Model Interface for Nano-Biosensing Application," *Solid State Electron*, vol. 195, p. 108374, 2022, doi: https://doi.org/10.1016/j.sse.2022.108374.

[36] K. Hagiya, A. Miyagawa, S. Nagatomo, and K. Nakatani, "Direct Quantification of Proteins Modified on a Polystyrene Microparticle Surface Based on ζ Potential Change," *Anal Chem*, vol. 94, no. 16, pp. 6304–6310, Apr. 2022, doi: 10.1021/acs.analchem.2c00457.

[37] L. Restrepo-Pérez, C. Joo, and C. Dekker, "Paving the way to single-molecule protein sequencing," *Nat Nanotechnol*, vol. 13, no. 9, pp. 786–796, 2018, doi: 10.1038/s41565-018-0236-6.

[38] S. Koch, P. Woias, L. K. Meixner, S. Drost, and H. Wolf, "Protein detection with a novel ISFET-based zeta potential analyzer," *Biosens Bioelectron*, vol. 14, no. 4, pp. 413–421, 1999, doi: https://doi.org/10.1016/S0956-5663(99)00008-1.